Fast 3D gradient shimming by only 2×2 pixels in XY plane for NMR-solution samples

Guangcao Liu, Xiaobo Qu, Shuhui Cai, Zhiyong Zhang, Zhiwei Chen, Congbo Cai, Zhong Chen*

Department of Electronic Science, Fujian Provincial Key Laboratory of Plasma and Magnetic Resonance, State Key Laboratory of Physical Chemistry of Solid Surfaces, Xiamen University, Xiamen, Fujian 361005, China

Abstract

Shimming is an essential process for most NMR experiments, and time saving in this process is desired. Here we propose a fast 3D gradient shimming with a low resolution of only 2×2 pixels in the XY plane, and the number of pixels in the Z direction remains unchanged. The proposed pulse sequences employ the selective excitation and the convection compensation. Consequently, the fast 3D gradient shimming adapts to a wide range of samples on regular NMR spectrometers.

***Keywords**:* Automatic shimming; 2×2 pixels; Regularization; Proton shimming; Thermal convection; Solution sample.

* Corresponding author. Phone: +86 592 2181712. Fax: +86 592 2189426. E-mail address: chenz@xmu.edu.cn.

1. Introduction

Gradient shimming is based on the field map method [1] to measure magnetic field distributions in samples. It optimizes shim currents to fit the magnetic inhomogeneity. The 3D gradient shimming was originally implemented on MRI scanners [2, 3]. In 1994, van Zijl provided a ^{1}H 3D gradient shimming method on NMR spectrometers [4]. Subsequently, Sukumar developed ^{2}H 1D gradient shimming [5]. In 2006, Weiger provided the TopShim method, which generated better spectral line shapes [6, 7]. Recently, Nishiyama suggested the gradient shimming on magic angle spinning samples [8]. These achievements have expanded the applicable range and improved the quality of gradient shimming. However, the 3D gradient shimming depended on high resolutions, e.g. 32×32×128 voxels, corresponding to 32×32×2=2048 scans. A large number of scans limited the speed of 3D gradient shimming.

Nowadays, the major shimming method for sample-to-sample shimming is the 1D gradient shimming [9, 10], which only optimizes on-axis shim coils, namely Z1 to Z7. However, it is sometimes necessary to optimize off-axis shims, such as X1, Y1, XZ, and YZ. This process is carried out by a search algorithm based on lock signals or peak areas. Unfortunately, it is difficult to predict when the off-axis shimming should be performed. Therefore, the maintenance shimming is recommended for off-axis shims in regular periods, monthly, weekly, or even more frequently [9].

The 3D gradient shimming is the most efficient method to optimize all shim coils. In 2004, Korostelev pioneered to reduce the number of pixels to 4×4 in the XY plane, and achieved both ^{1}H and ^{2}H 3D shimming with the modified PFGSTE pulse

sequence [11]. The pulse sequence contained three 90°-RF pulses that required a long repetition time (TR), rendering the scan time longer than 1 minute in each iteration. This method cannot adapt to fewer pixels such as 2×2 and 3×3 (see Table 6.3 in Ref. [11]). In following sections, we demonstrate that both 2×2 and 3×3 pixel approaches are applicable for 3D gradient shimming.

2. Methods

A rapid 3D gradient shimming can benefit from low resolutions in the XY plane. For the purpose of avoiding under-determination, the order of X in off-axis shim coils should be smaller than the number of pixels in the X direction, as well as in the Y direction. Table 1 summarizes that high-order off-axis shim coils should be excluded for shimming with 2×2 pixels or 3×3 pixels. Previously-recorded optimized shim values are loaded prior to shimming to overcome the deficiency of excluding these high-order shim coils. Conventional high-resolution approaches are in the risk of the phase-encoding current overflow, when phase encoding is generated by current-constrained X1 and Y1 shim coils. Both 2×2 and 3×3 pixel approaches significantly reduce the maximum phase-encoding gradients to protect X1 and Y1 shim currents.

Table 1 Shim coils available in 1×1 pixel (1D), 2×2 pixel (3D) and 3×3 pixel (3D) gradient shimming. The 1D gradient shimming is regarded as the special case having 1×1 pixel in the XY plane. A Varian 28-shim set is used as an example, and Z0 shim coil is not included.

Number of pixels	X order	Y order	Shim coils in the available order	Shim coils out of the available order
1×1	0 order	0 order	Z1, Z2, Z3, Z4, Z5, Z6, Z7	Other shim coils
2×2	⩽1st order	⩽1st order	Z1, Z2, Z3, Z4, Z5, Z6, Z7, X1, Y1, XZ, YZ, XY, XZ2, YZ2, ZXY, Z3X, Z3Y, Z2XY, Z4X, Z4Y	X3, Y3, ZX3, ZY3, X2Y2,ZX2Y2,Z2X2Y2
3×3	⩽2nd order	⩽2nd order	Z1, Z2, Z3, Z4, Z5, Z6, Z7, X1, Y1, XZ, YZ, XY, XZ2, YZ2, ZXY, Z3X, Z3Y, Z2XY, Z4X, Z4Y, X2Y2, ZX2Y2, Z2X2Y2	X3, Y3, ZX3, ZY3

Low-resolution approaches should make full use of every pixel. Hence the FOV in the XY plane is only slightly larger than the sample size. If there is a small deviation of the FOV center, the alias takes place, as illustrated in Fig. 1b. Such deviation is caused by two factors. First, the center of the X1 and Y1 shim gradients, i.e. the phase-encoding gradients, does not coincide with that of the sample. Second, the mismatch of indices in Fourier transform induces an extra amount. The 2 pixels along the X direction correspond to symmetric position x_{id} = [-1/2, 1/2] in the image, but in normal Fourier transform x_{id} = [0, 1] induces 1/2 pixel deviation of x_{id} in the image. In this case, shifting a floating number of pixels, e.g. 0.27 pixel, is based on the

frequency-shift property of Fourier transform, namely,

$$I(x_{id} + D_x) = FT[S(k_x)e^{-iD_x k_x}], \quad (1)$$

where D_x denotes the deviation of the gravity center along the X direction; S is the acquired signal; k_x is the index of the acquired signal; I is the image value; and x_{id} is the index of a pixel in the image. The center correction is repeated several times to ensure that the deviation becomes inconspicuous in the image, e.g. $D_x \leq 0.01$ pixel. This data process is accomplished by the 3D gradient shimming program in VnmrJ.

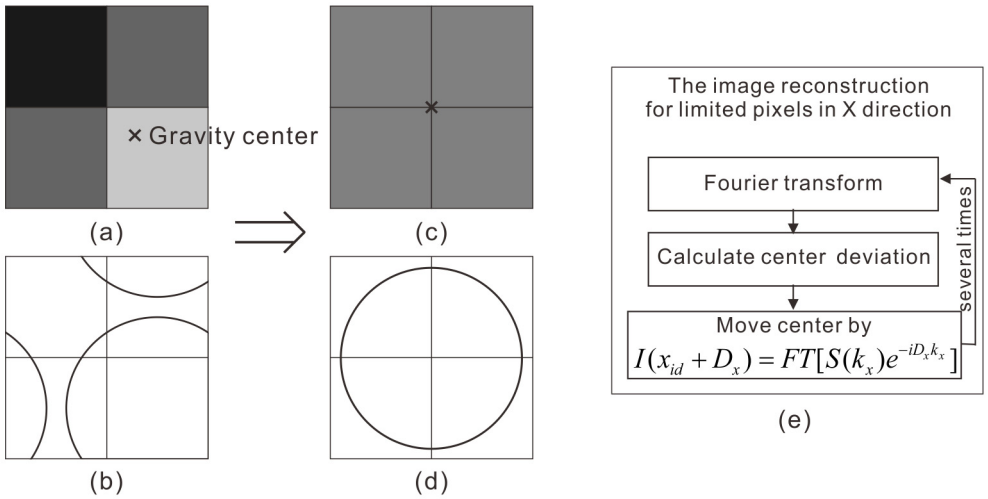

Fig. 1. (a) The image with different intensities in different regions after Fourier transform, (b) an illustration of the sample deviating from the FOV center, (c) the image with uniform intensity after correction, (d) an illustration of the sample located at the FOV center, and (e) the image reconstruction process.

A fast speed is achieved by 2×2 pixels using the gradient echo sequence with a short TR and accordingly a small flip angle. The scan time of ^{1}H 3D gradient shimming can be reduced from longer than 1 min to shorter than 1 s per iteration. Since the sensitivity of ^{1}H signals is 100 times higher than that of ^{2}H signals [5], a small portion of protons in the sample is sufficient. The ^{2}H 3D gradient shimming

may require more scans and a longer TR than the ^{1}H shimming, and the scan time is reduced to 4 ~ 20 s per iteration with 1 ~ 4 averages. In practice, it is recommended to try the ^{1}H approach first.

The proposed pulse sequences are shown in Fig. 2. They inherit Bruker 3D gradient shimming sequence with phase encoding by the X1 and Y1 shim gradients, which only change at the beginning and at the end of every scan to overcome the time-lagging control of the X1 and Y1 shim coils [10, 12]. A spoil gradient is required to dephase the residual transverse magnetizations for the 2×2 pixel approach. Conventional high-resolution 3D shimming requires strong phase-encoding gradients, which may interfere with the selective excitation. This interference is resolved by 2×2 pixels, because phase-encoding gradients in low-resolution 3D shimming are quite weak. Moreover, a large frequency-encoding bandwidth in the sequence can further reduce chemical artifacts in the image.

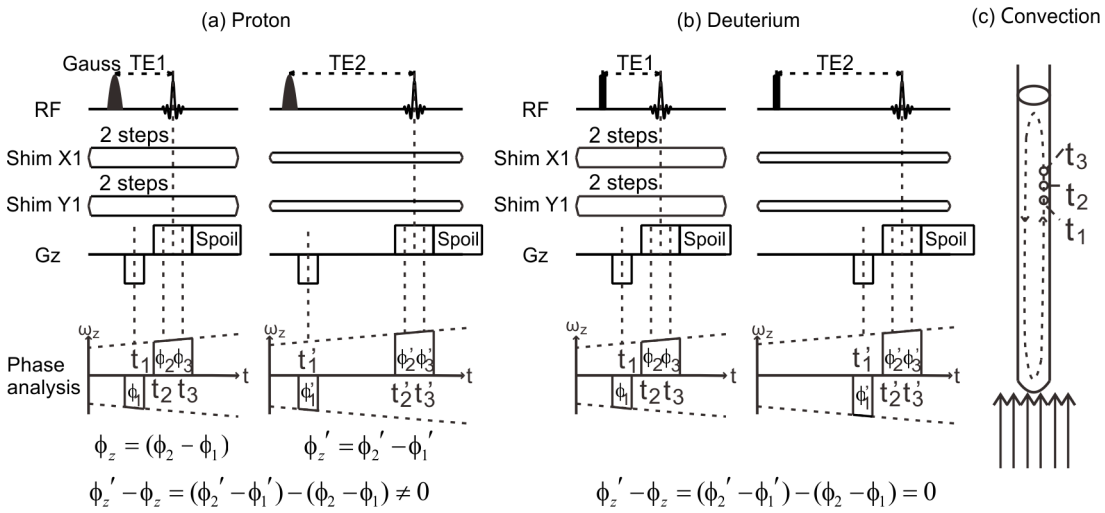

Fig. 2. (a) ^{1}H pulse sequence with a Gaussian RF pulse. (b) ^{2}H pulse sequence with a hard RF pulse. The separations of dephased and readout gradients are different between ^{1}H and ^{2}H sequences. (c) Thermal convection in the sample caused by the VT airflow. When a magnetization

moves upward, $\omega_z(t)=\gamma\times(\pm g_z)\times z(t)$ increases along with z(t). Consequently, areas of the $\omega_z(t)$ plot such as ϕ_1, ϕ_2, ϕ_1', and ϕ_2' are trapezoidal.

A defect is related to thermal convection [13]. Evans and co-authors suggested the convection compensation in 1D gradient shimming [14]. In the ^{1}H sequence (Fig. 2a), the dephaser ($-G_z$) is separated from the readout gradient to suppress radiation damping, rendering $\phi_z'-\phi_z\neq 0$. Therefore, the ^{1}H sequence suffers from the thermal convection. On the contrary, the ^{2}H sequence does not, because of $\phi_z'-\phi_z=0$. The double-echo sequence is a conventional method to compensate the convection, such as double-gradient-echo, double-spin-echo, and double-stimulated-echo sequences [15, 16]. Two proposed ^{1}H sequences shown in Fig. 3 implement double-gradient echoes.

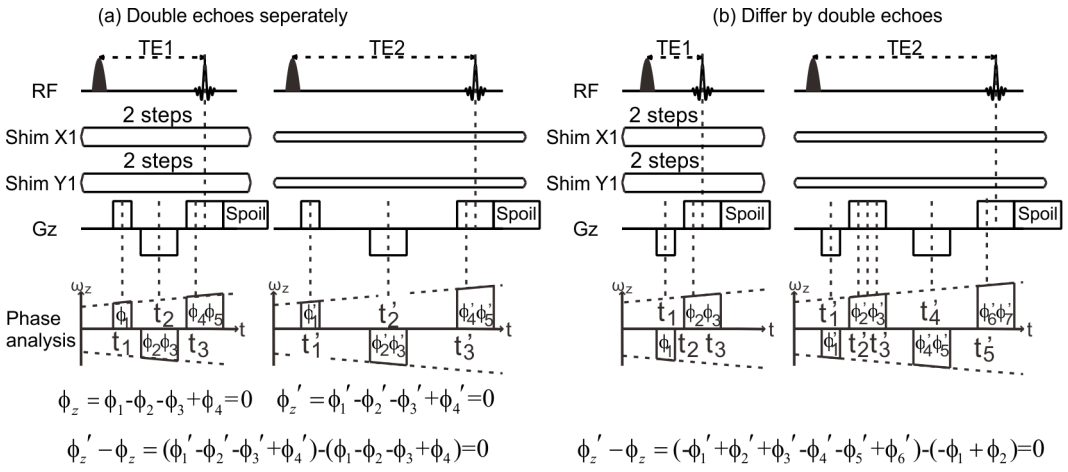

Fig. 3. Two improved ^{1}H sequences to compensate thermal convection. (a) Both two imaging scans utilize the double gradient echoes; (b) two imaging scans differ by double gradient echoes.

3. Experiments and Results

3.1 Experimental details

Experiments were carried out on a Varian 500 MHz NMR spectrometer, which

was equipped with the Varian 28-shim set. The software VnmrJ supplied the *gmapxyz* application for 3D gradient shimming. We modified the default sequence into the proposed ^{1}H sequences in Fig. 3b and the ^{2}H sequence in Fig. 2b. The two convection compensation ^{1}H sequences in Fig. 3 yield close shimming results. The default setting contained 4×4 pixels, 6×6 pixels, and 8×8 pixels. We added 1×1 pixel, 2×2 pixels, and 3×3 pixels. An integration of 1×1 pixel facilitated the maintenance of both 1D and 3D shimming programs. Furthermore, Z7 shim coil was not included for the ill-posed problem [17, 18]. Table 2 displays parameters used in the present study. A flow chart of the selective 3D gradient shimming is shown in Fig. 4. Redundant delays in *gmapxyz* are removed.

In the data process of *gmapxyz*, the field map vector $\mathbf{b}$ only counts the inhomogeneous part $\mathbf{b}_{\text{inho}} = \mathbf{b} - \mathrm{b}_0\mathbf{I}$, in which b_0 is the average value of $\mathbf{b}$ and $\mathbf{I}$ is the vector filled with "ones". Also, the shim map matrix $\mathbf{A}$ only counts the inhomogeneous part $\mathbf{A}_{\text{inho}} = \mathbf{A} - \mathbf{A}_0$, in which $\mathbf{A}_0$ is made up of average shim-map values. Consequently, the fitting $\min(|\mathbf{A}_{\text{inho}}\mathbf{x} - \mathbf{b}_{\text{inho}}|)$ may result in a small RF-frequency deviation in the next iteration. In experiments, we calibrate the RF frequency with the *Adjust offset* button in every iteration to reduce this deviation.

Table 2 Parameters for tests.

Parameter	Selective ^{1}H	^{2}H
Soft-pulse width (ms)	1~5	/
Bandwidth (kHz)	100	3
Z-axis pixels	64 or 128	64 or 128
XY FOV (mm)	5×5	5×5
TE1 (ms)	8	50
TE2-TE1 (ms)	25~30	150~200
Repetition time (s)	0.1	0.4~0.6
Flip angle (°)	5~20	15~30
Dummy scans	1~2	1~2
Number of averages	1	1, 4, 8 or more

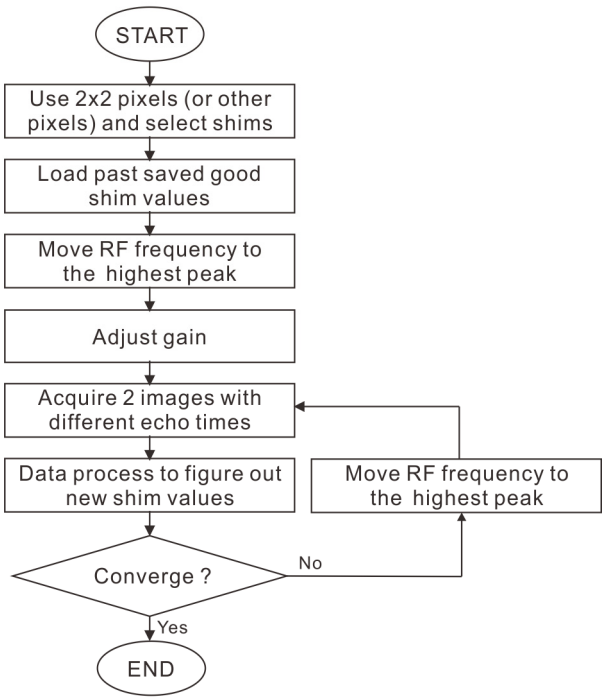

Fig. 4. Flow chart of the 3D gradient shimming.

3.2 Results

3.2.1 Tests for offsetting shim coils

These tests starts from an optimal shimming result. Then, each shim current is changed by a certain amount. Through 2×2 pixel gradient shimming, the full width at half maximum (FWHM) of tetramethylsilane (TMS) peak is restored step by step, as shown in Fig. 5. Similar results are obtained when other shim coils, such as XZ2, YZ2, and ZXY, are tested. If the initial homogeneity is inferior, it is necessary to use a short echo delay ($\Delta TE = TE2 - TE1$).

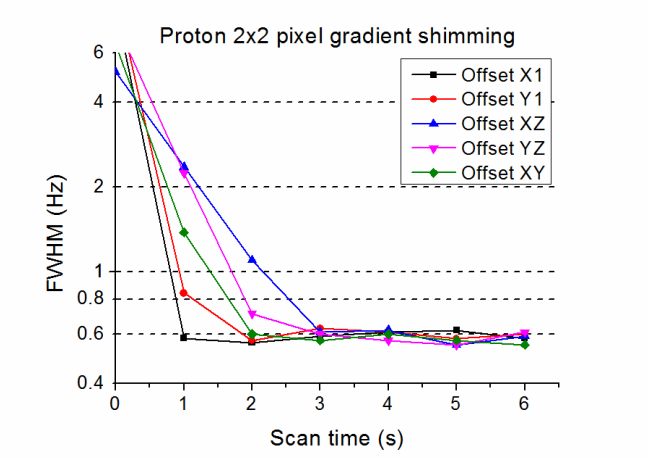

Fig. 5. Results of 2×2 pixel ^{1}H gradient shimming that is initialized by offsetting one of off-axis shim coils. The test sample is the mixture of DMSO (500 μL) and DMSO-d_6 (100 μL) containing 0.05% TMS.

3.2.2 Tests for various pixels

Tests of both ^{2}H and ^{1}H shimming start from 5 different previously-recorded optimized shim values, which have been obtained from different samples for longer than one year. Figure 6 shows the FWHM results of the ^{2}H gradient shimming with 1×1 pixel, 2×2 pixels, 3×3 pixels and 6×6 pixels on the standard ^{1}H line shape sample

(1% $CHCl_3$ in acetone-d_6). Figure 7 shows the FWHM results of ^1H gradient shimming with 2×2 pixels and 6×6 pixels on the doped 4 Hz H_2O/D_2O sample (0.1 mg/ml $GdCl_3$, 0.1% DSS in 20% H_2O in D_2O). In these figures, shimming results of 2×2 pixel and 3×3 pixel approaches are very close to those of the 6×6 pixel counterpart. By contrast, the FWHMs of 1D gradient shimming (i.e. 1×1 pixel) shown in Fig. 6a are wider than 1 Hz. Therefore, the 1D approach requires an extra shimming on off-axis shim coils.

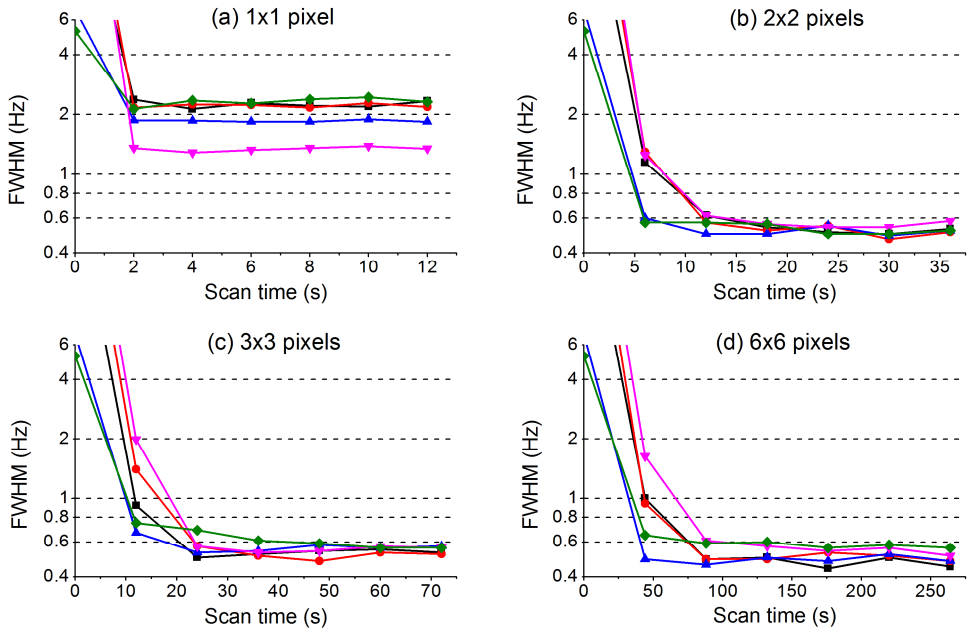

Fig. 6. The ^2H gradient shimming with various pixels on the standard ^1H line shape sample. The line dotted with (■) is initiated from the previous optimal shim value of a ^1H standard line shape sample saved 1 year and 9 months ago. The line with (●) is initiated from the shim value of an n-butyl bromide sample saved 1 year and 7 months ago. The line with (▲) is initiated from the shim value of a ^1H standard sensitivity sample saved 1 year and 4 months ago. The line with (▼) is initiated from the shim value of a D_2O sample saved 2 years and 4 months ago. The line with (◆) is initiated from the shim value of a pure H_2O sample saved 1 year and 3 months ago.

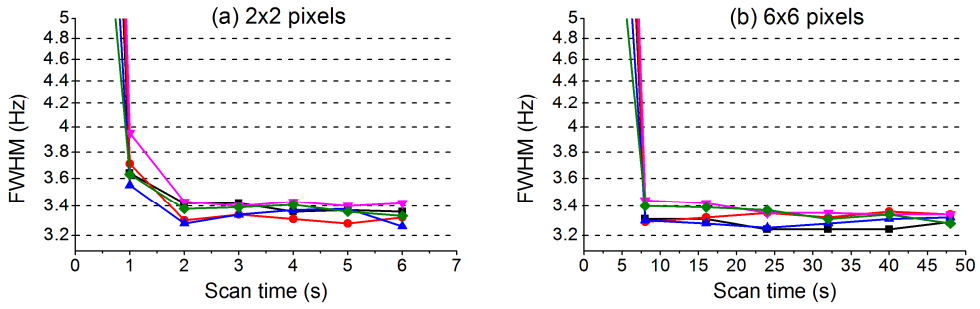

Fig. 7. The ^{1}H gradient shimming with 2×2 pixels and 6×6 pixels on the doped 4 Hz H_2O/D_2O sample. Lines dotted with (■), (●), (▲), (▼), and (◆) are initialized from the same shim values as those used in the ^{2}H shimming (Fig. 6).

3.2.3 Tests for short samples in sample-to-sample shimming

The 2×2 pixel approach is expected to generate higher homogeneity than 1D gradient shimming for short samples, because more shim coils are included. The initial shim values are optimized on the 500 μL sample. Then, 1D ^{2}H gradient shimming and the 2×2 pixel ^{2}H approach work well on 500 μL and 800 μL samples. When short samples (400 μL and 350 μL D_2O) are tested, FWHMs for 1D approach degenerate to 1.01 Hz and 3.35 Hz, but FWHMs for 2×2 pixel approach are acceptable 0.61 Hz and 0.82 Hz (Table 3).

Table 3 FWHMs of the trimethylsilyl propionate (TSP) peak after ^{2}H gradient shimming for different volumes of D_2O solvent.

Volume	1×1 pixel	2×2 pixels
800 μL	0.64 Hz	0.66 Hz
500 μL	0.52 Hz	0.59 Hz
400 μL	1.01 Hz	0.61 Hz
350 μL	3.35 Hz	0.82 Hz

3.2.4 Comparison between 3D 2×2 pixel shimming and 1D + off-axis shimming.

A comparison between the 2×2 pixel ^{1}H gradient shimming and the 1D ^{1}H gradient shimming + low-order off-axis auto shimming is shown in Table 4. The low-order off-axis auto shimming is based on two approaches, i.e. lock signals and FID areas. It takes about 3.5 mins for lock-signal optimization and about 1.5 mins for FID-area optimization in every iteration, following an optimal searching order of [X1, Y1, XZ, X1, YZ, Y1, Z1] with the *Proshim* method [9]. Sometimes, 2 iterations of 1D + low-order off-axis shimming are required. The 2×2 pixel ^{1}H shimming is almost as fast as 1D ^{1}H gradient shimming. It takes 3~4 s in every iteration for both 2×2 pixel and 1D shimmings, including setting up parameters, scanning, data process, and loading shimming currents. The RF frequency calibration takes additional 3~4 s in every iteration. Clearly, (a) the 2×2 pixel approach is faster than 1D gradient shimming + low-order off-axis shimming. The more shim coils to be optimized there are, the longer time it takes for the searching process. (b) Most shimming results are comparable between the 2×2 pixel approach and 1D + lock optimization of low-order off-axis shims. (c) When the lock optimization is replaced with ^{1}H FID-area optimization, results of low-order off-axis auto shimming degenerate. Apparently, the ^{1}H FID-area optimization is unsuitable to multiple strong peak solvents.

Table 4 Comparison between 2×2 pixel gradient shimming and 1D + off-axis shimming. A~E are initial shim values that have been saved for a long time. The test sample is the mixture of propyl alcohol (60 μL) and acetone-d_6 (340 μL) containing 0.03% TMS. Results are measured on FWHMs of the TMS peak.

Initial fields	A	B	C	D	E
2×2 pixel approach	0.59	0.63	0.56	0.62	0.55
1D + off-axis lock optimization	0.60	0.57	0.62	0.58	0.63
1D + off-axis FID-area optimization	1.29	1.03	1.03	0.63	0.88

3.2.5 Tests for ^1H shimming on a sample with multiple strong peaks

The center frequency of the selective excitation is moved toward the highest peak by default. Figure 8 shows that the FWHM of the TMSP peak is acceptable after selective 2×2 pixel gradient shimming.

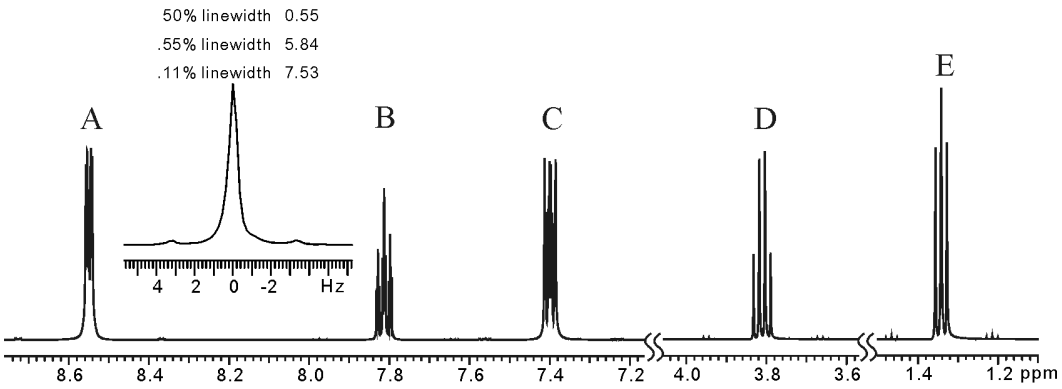

Fig. 8. A ^1H NMR spectrum obtained from selective 2×2 pixel ^1H gradient shimming. The test sample is the mixture of pyridine (150 μL) and alcohol (50 μL) in D_2O (200 μL) containing 0.05% TMSP. The FWHM of the TMSP peak after shimming is 0.55 Hz in the inset graph. The center frequency of the selective RF pulse can be moved to any peak among A ~ E.

3.2.6 Tests for ^1H shimming under thermal convection

Shimming is carried out when the temperature of the sample is stable. Results in Fig. 9 are measured on FWHMs of the TMS peak. When the original ^1H gradient echo

sequence is tested (Fig. 2a) on the acetone solvent, the FWHM-temperature curve displays a "√". The temperature for the best shimming result is close to 25 °C, which is the value in the absence of airflows. Either cool or warm airflows lead to degenerated results. On the contrary, when flow-compensated gradients in Fig. 3a or Fig. 3b are used, shimming results are unaffected by the thermal convection. The FWHMs remain stable around 0.5 Hz. The thermal-convection phenomenon is more pronounced in the acetone solvent than in the DMSO solvent.

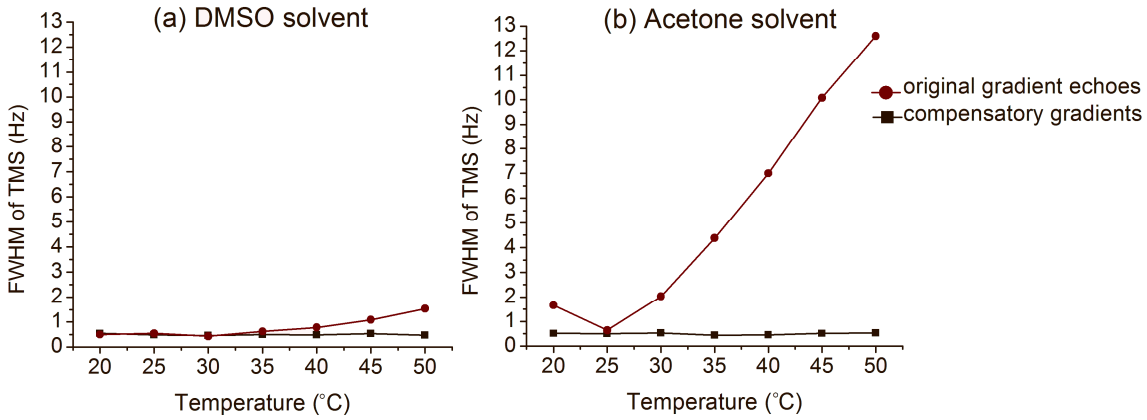

Fig. 9. Thermal convection test for ^{1}H 2×2 pixel gradient shimming on (a) DMSO solvent and (b) acetone solvent.

4. Discussion

Results demonstrate that 2×2 pixel and 3×3 pixel3D gradient shimming converges in a few iterations through starting from previously-recorded optimized shim values. The proposed shimming method is unaffected by chemical artifacts and thermal convections.

The oscillations of result FWHMs in Figs. 5, 6, and 7 are caused by some factors, such as shim map errors, field map errors, condition changes, and ill-posed problems.

An expression is given [18, 19] to disclose the relationship between these factors,

$$\|\delta\mathbf{r}\| \leq \|\delta\mathbf{A}\| \cdot \|\mathbf{x}\| + \|\delta\mathbf{b}\| + \frac{\|\delta\mathbf{A}\|}{\|\mathbf{A}\|} \mathrm{K}(\mathbf{A}) \|\mathbf{r}\|, \quad (2)$$

where $\mathbf{r}$ is the residual inhomogeneity when no errors are present ($\mathbf{r} = \mathbf{Ax} - \mathbf{b}$); $\delta\mathbf{r}$ is the residual error; $\delta\mathbf{b}$ is the field map error; and $\mathrm{K}(\mathbf{A})$ is the condition number of the ill-posed problem. The residual $\mathbf{r}$ includes condition changes. For the last term $\frac{\|\delta\mathbf{A}\|}{\|\mathbf{A}\|} \mathrm{K}(\mathbf{A}) \|\mathbf{r}\|$, the shim map error $\|\delta\mathbf{A}\|$ and the residual inhomogeneity $\|\mathbf{r}\|$ are amplified by ill-posed $\mathrm{K}(\mathbf{A})$. Consequently, the $\|\delta\mathbf{r}\|$ results in oscillations. Therefore, it is important to reduce the ill-posed problem through using a regularization method or excluding some high-order shim coils.

The low resolution cannot be applied to the strong inhomogeneity in X and Y directions. Typically, ΔTE is 25 ms (corresponding 40 Hz) in ^{1}H gradient shimming. The inhomogeneity between 2 pixels in the X direction should be less than 40 Hz /2 =20 Hz to avoid phase wrap. By contrast, for the conventional high resolution of 32 pixels, the inhomogeneity in the X direction can be 20×32 = 640 Hz. Therefore, the allowed inhomogeneity of 2 pixels is much smaller than that of 32 pixels. When shimming starts from previously-recorded optimized shim values, the maximum 20 Hz inhomogeneity for 2 pixels is sufficient, since there exists only 2~3 Hz inhomogeneity in the X and Y directions shown in results of 1D gradient shimming (Fig. 6a). The shim mapping process imposes a large inhomogeneity by offsetting each shim coils. However, it should not exceed the maximum 20 Hz for mapping X1, Y1 and XY shim coils.

5. Conclusions

We have presented a fast 3D gradient shimming based on the low resolution in the XY plane. The merit of this shimming method is that off-axis shim coils can be immediately optimized for routine NMR experiments.

Acknowledgments

This work is supported by the NNSF of China under Grants (11174239, 61201045 and 11275161). The authors thank Professor Tim (Tien Mo) Shih for linguistic assistance and Dr. Birong Zeng for her support to experiments.

References

[1] A.A. Maudsley, H.E. Simon, S.K. Hilal, Magnetic-field measurement by NMR imaging, J. Phys. E 17 (1984) 216-220.

[2] M.G. Prammer, J.C. Haselgrove, M. Shinnar, J.S. Leigh, A new approach to automatic shimming, J. Magn. Reson. 77 (1988) 40-52.

[3] P. Webb, A. Macovski, Rapid, fully-automatic, arbitrary-volume in vivo shimming, Magn. Reson. Med. 20 (1991) 113-122.

[4] P.C.M. Van Zijl, S. Sukumar, M.O. Johnson, P. Webb, R.E. Hurd, Optimized shimming for high-resolution NMR using three-dimensional image-based field-mapping, J. Magn. Reson. A 111 (1994) 203-207.

[5] S. Sukumar, M.O. Johnson, R.E. Hurd, P.C.M. vanZijl, Automated shimming

for deuterated solvents using field profiling, J. Magn. Reson. 125 (1997) 159-162.

[6] M. Weiger, T. Speck, M. Fey, Gradient shimming with spectrum optimisation, J. Magn. Reson. 182 (2006) 38-48.

[7] M. Weiger, M. Fey, T. Speck, Method for automatic shimming for nuclear magnetic resonance spectroscopy, US Patent 7,605,589 (2008).

[8] Y. Nishiyama, Y. Tsutsumi, H. Utsumi, Magic shimming: gradient shimming with magic angle sample spinning, J. Magn. Reson. 216 (2012) 197-200.

[9] R. Crouch, Shimming with VnmrJ 3.1 software for peak NMR performance, Agilent Technology, (2011) 1-7.

[10] M. Weiger, T. Speck, Shimming for high-resolution NMR spectroscopy, eMagRes, (2011) 4468-4486.

[11] V.V. Korostelev, Improvements in three-dimensional automated shimming techniques in high-resolution nuclear magnetic resonance, Ph.D. Thesis, Manchester University, 2004.

[12] M. Weiger, D. Moskau, R. Kerssebaum, W.E. Hull, Gradient shimming: principles and practical aspects, Bruker Spin Report (2005) 1-27.

[13] A. Jerschow, Thermal convection currents in NMR: flow profiles and implications for coherence pathway selection, J. Magn. Reson. 145 (2000) 125-131.

[14] C.L. Evans, G.A. Morris, A.L. Davis, A new method for variable temperature gradient shimming, J. Magn. Reson. 154 (2002) 325-328.

[15] P. T. Callaghan, ‘‘Principles of Nuclear Magnetic Resonance Microscopy,’’ Oxford Univ. Press, Oxford, 1993.

[16] A. Jerschow, N. Müller, Suppression of convection artifacts in stimulated-echo diffusion experiments. Double-stimulated-echo experiments, J. Magn. Reson. 125 (1997) 372-375.

[17] P.C. Hansen, Regularization tools: a matlab package for analysis and solution of discrete ill-posed problems, Numer. Algorithms, 6 (1994) 1-35.

[18] D.H. Kim, E. Adalsteinsson, G.H. Glover, D.M. Spielman, Regularized higher-order in vivo shimming, Magn. Reson. Med. 48 (2002) 715-722.

[19] P.A. Wedin, Perturbation theory for pseudo-inverses, BIT. 13 (1973) 217-232.